

RESEARCH PAPER

## The preparation, structural characterization, optical properties, and antibacterial activity of the CuO/Cu<sub>2</sub>O nanocomposites prepared by the facile thermal decomposition of a new copper precursor

Aliakbar Dehno Khalaji <sup>1\*</sup>, Marketa Jarosova <sup>2</sup>, Pavel Machek <sup>2</sup>

<sup>1</sup>Department of Chemistry, Faculty of Science, Golestan University, Gorgan, Iran

<sup>2</sup>Institute of Physics, Czech Academy of Sciences, Na Slovance 2, 182 21 Prague, Czech

### ABSTRACT

**Objective(s):** In this study, a new copper precursor was prepared from the combination of Cu(CH<sub>3</sub>COO)<sub>2</sub>·H<sub>2</sub>O (1 g in 5 ml of methanol) and benzoic acid (1 g in 5 ml of methanol) at room temperature. Following that, the copper precursor was calcined at the temperature of 500°C and 600°C for 1.5 hours to form CuO/Cu<sub>2</sub>O nanocomposites with the code numbers of CuO-1 and CuO-2, respectively.

**Materials and Methods:** The prepared CuO/Cu<sub>2</sub>O nanocomposites were characterized by Fourier Transform infrared (FT-IR), UV-Vis, and photoluminescence (PL) spectroscopy, X-ray powder diffraction (XRD), and transmission electron microscopy (TEM).

**Results:** The results of the FT-IR and XRD techniques confirmed the formation of the CuO/Cu<sub>2</sub>O nanocomposites. In the UV-Vis of CuO/Cu<sub>2</sub>O nanocomposites, two peaks were observed at approximately 216 and 277 nanometers, which were assigned to the direct transition of electrons and surface plasmon resonance. In addition, the TEM images indicated that the CuO/Cu<sub>2</sub>O nanocomposites had diverse shapes with high agglomeration. The antibacterial results also showed that the inhibitory effects of the prepared CuO/Cu<sub>2</sub>O nanocomposites (CuO-1 and CuO-2) were more significant against the two gram negative strains compared to the two gram positive strains.

**Keywords:** Antibacterial, Copper precursor, CuO/Cu<sub>2</sub>O nanocomposites, Photoluminescence

### How to cite this article

Dehno Khalaji AA, Jarosova M, Machek P. The Preparation, structural characterization, optical properties, and antibacterial activity of the CuO/Cu<sub>2</sub>O nanocomposites prepared by the facile thermal decomposition of a new copper precursor. *Nanomed J.* 2020; 7(3): 231-236. DOI: 10.22038/nmj.2020.07.0007

### INTRODUCTION

Recently, researchers have paid special attention to the preparation, characterization, and consideration of the physical, chemical, and antibacterial properties of various transition metal oxide nanostructures, such as Fe<sub>2</sub>O<sub>3</sub> [1], NiO [2], Mn<sub>3</sub>O<sub>4</sub> [5], CeO<sub>2</sub> [4], Co<sub>3</sub>O<sub>4</sub> [5], and CuO [6-8]. Among these nanostructures, copper oxides (CuO and Cu<sub>2</sub>O) are widely known as p-type semiconductors with narrow band gaps of 1.2 and 2 eV, respectively [9]. Among the other beneficial properties of these elements are the excellent chemical stability, cost-efficiency, abundance and facile preparation [10, 11]. Therefore, they

have gained importance for antibacterial [12], and optical applications [13], and dye removal adsorption [14]. The sensitivity of the activity of these elements is closely associated with the redox activation of copper ions. Several studies have been focused on the preparation of CuO/Cu<sub>2</sub>O composite material [9, 15-17]. For instance, Zhang *et al.* fabricated a CuO/Cu<sub>2</sub>O composite microframe through top-down oxidation etching, and the composite showed more enhanced CO sensing performance compared to the pure Cu<sub>2</sub>O and CuO [9]. Moreover Lv *et al.* synthesized a novel thin film assembled by CuO/Cu<sub>2</sub>O nanosheets on a Cu foil, with the CuO/Cu<sub>2</sub>O nanosheets functioning as the active materials for the detection of glucose [15]. In another research, Sahu *et al.* reported the enhanced catalytic activity of CuO/Cu<sub>2</sub>O in

\* Corresponding Author Email: [alidkhalaji@yahoo.com](mailto:alidkhalaji@yahoo.com)

Note. This manuscript was submitted on March 2, 2020; approved on May 28, 2020

the reduction of 4-nitrophenol [16]. On the other hand, Yang et al.

synthesized porous CuO/Cu<sub>2</sub>O composites based on their superior catalytic performance in CO oxidation [17].

In the present study, the optical and antibacterial activity of CuO/Cu<sub>2</sub>O nanocomposites prepared by the calcination of the combination of Cu(CH<sub>3</sub>COO)<sub>2</sub>·H<sub>2</sub>O and benzoic acid (weight ratio 1:1) at the temperature of 500°C and 600°C were synthesized, characterized and evaluated..

## MATERIALS AND METHODS

All the chemical reagents were purchased from Merck Company (Germany). and used without further purification. The Fourier-transform infrared (FT-IR) spectra were recorded as a KBr disk on an FT-IR Perkin–Elmer spectrophotometer. Optical absorption measurements were performed using a UV-Vis spectrophotometer within the wavelength range of 200–800 nanometers at room temperature. In addition, the photoluminescence (PL) emission spectra were performed using the Hitachi F4500 spectrofluorometer. The X-ray diffraction (XRD) patterns of the complexes were obtained on the Empyrean powder diffractometer of PANalytical in Bragg-Brentano configuration, which was equipped with a flat sample holder and PIXCel3D detector (Cu K $\alpha$  radiation,  $\lambda = 1.5418 \text{ \AA}$ ). The transmission electron microscopy (TEM) images of the nanoparticles were also recorded using a transmission electron microscope (model: Philips CM120) with a LaB<sub>6</sub> cathode, operating at 120 kV and equipped with a CCD camera (Olympus Veleta).

### Antibacterial activity

Antibacterial tests were carried out using two pure, gram-negative bacterial strains (*E. coli* and *S. aureus*) and two gram-positive strains (*P. aeruginosa* and *B. cereus*). To estimate the antibacterial activity of the CuO/Cu<sub>2</sub>O nanocomposites, the well diffusion assay was performed based on the study by Sharmila et al. [18]. To this end, a uniform culture of the bacteria was prepared on the agar medium, and 0.05 gram of the CuO nanoparticles was dispersed in five milliliters of distilled water. The discs of the samples and antibiotics were placed on plates at appropriate distances and incubated at the temperature of 37°C for 24 hours for the assessment of the growth inhibitory zone formation.

### Preparation of the CuO/Cu<sub>2</sub>O nanocomposites

A solution was prepared composed of one gram of Cu(CH<sub>3</sub>COO)<sub>2</sub>·H<sub>2</sub>O in five milliliters of methanol, which was combined with another solution of containing one gram of benzoic acid in five milliliters of methanol, and the mixture was stirred for approximately 10 minutes. The solvent was evaporated, and the precipitates (copper precursor) were collected. Afterwards, one gram of the copper precursor was loaded on a quartz crucible and ground for five minutes. Finally, the copper precursor was placed inside a furnace. The temperature of the furnace increased by 20°C per minute, and the precursor was calcined at the temperature of 500°C and 600°C for three hours. The black product was washed with H<sub>2</sub>O/CH<sub>3</sub>OH (1:1 v/v), dried at the temperature of 80°C for three hours, and characterized using various techniques.

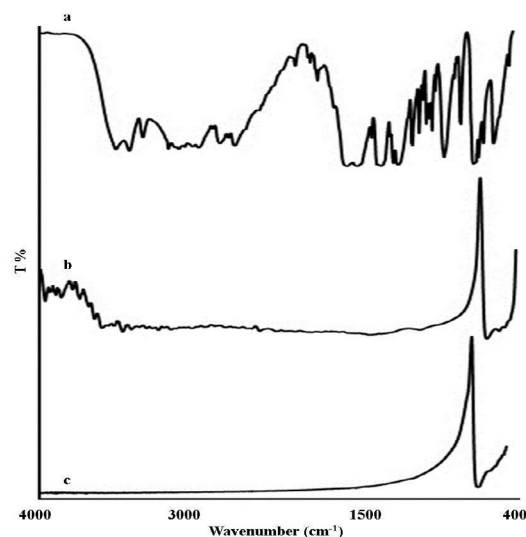


Fig 1. FT-IR spectra of a) Cu precursor, b) CuO-1 and, c) CuO-2

## RESULTS AND DISCUSSION

### FT-IR spectra

Fig 1 shows the FT-IR spectra of the copper precursor and prepared CuO/Cu<sub>2</sub>O nanocomposites at the temperature of 500°C (Cu-1) and 600°C (CuO-2). Several sharp peaks were observed in the FT-IR spectrum of the Cu precursor (Fig 1-a) which corresponded to C-H, C=O, C=C, and other groups. For instance, the sharp peaks at approximately 3,479, 3,374, 3,268 cm<sup>-1</sup> were assigned to the COO of the OH vibrations of benzoic acid and acetate ion. Moreover, the peaks observed at 1,682 and 1,602 cm<sup>-1</sup> were assigned to the C=O and C=C

groups. The peaks at approximately 3,071, 2,989, 2,885, and 2,835  $\text{cm}^{-1}$  indicated the presence of C-H aliphatic and aromatic.

After the calcination of copper precursor at the high temperature of 500°C and 600°C, the FT-IR spectra of the products were obtained (Figs 1-b, & 1-c). Four peaks were observed at approximately 635, 543, 497 and, 465  $\text{cm}^{-1}$  in the FT-IR spectrum of CuO-1 (Fig 1-b), and two peaks were observed at approximately 639, and 509  $\text{cm}^{-1}$  in the FT-IR spectrum of CuO-2 (Fig 1-c). Furthermore, the peaks appearing at 635  $\text{cm}^{-1}$  (CuO-1) and 639  $\text{cm}^{-1}$  (CuO-2) indicated the presence of Cu<sub>2</sub>O [19], which was also confirmed by the by XRD patterns [9, 15-17]. These findings confirmed the preparation of the CuO/Cu<sub>2</sub>O nanocomposites, which is consistent with the previous studies in this regard [15-17].

### UV-Vis spectra

The UV-Vis spectral analysis was applied as an important technique for the characterization of the electron transitions and surface plasmon resonance (SPR) property of the copper precursor and prepared CuO/Cu<sub>2</sub>O nanocomposites. Fig 2 depicts the UV-Vis spectra of the copper precursor and prepared CuO/Cu<sub>2</sub>O nanocomposites. In the copper precursor (Fig 2-a), a peak was observed at approximately 270 nanometers corresponded to the intraligand for benzoic acid and an extremely broad peak at about 770 nanometers, which corresponded to the d-d transition of the copper(II) ion.

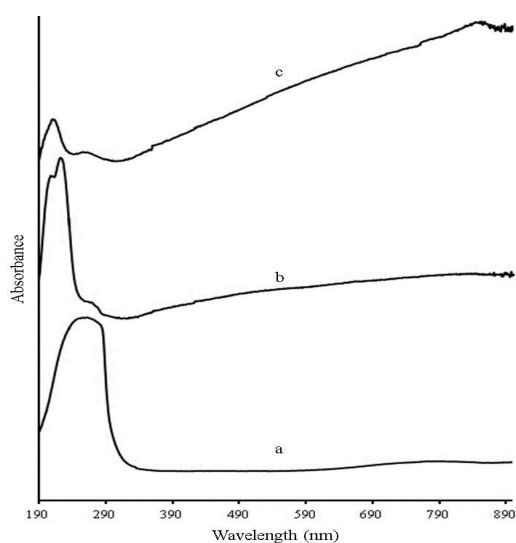


Fig 2. UV-Vis spectra of a) Cu precursor, b) CuO-1 and, c) CuO-2

The UV-Vis spectra of CuO-1 and CuO-2 (Figs 2-b & 2-c) clearly represented the characteristic peak corresponding to the adsorption edge of approximately 216 and 227 nanometers for CuO-1 and 216 nanometers for CuO-2 due to the direct transition of electrons [13]. Moreover, the peak appearing at approximately 277 nanometers clearly represented the SPR peak, which is in line with the previous findings regarding CuO nanoparticles [20].

### PL spectra

Fig 3 shows the PL spectra of the CuO/Cu<sub>2</sub>O nanocomposites (CuO-1 and CuO-2). The PL spectrum of CuO-1 consisted of four major peaks at approximately 323, 350, 415, and 632 nanometers (Fig 3-a), while CuO-2 consisted of three peaks at 322, 348, and 627 nm (Fig 3-b).

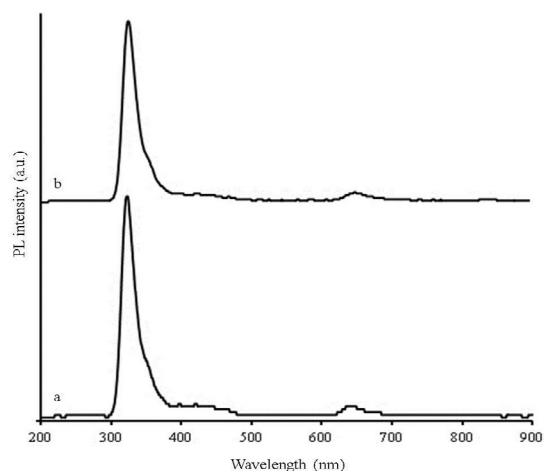


Fig 3. PL spectra of a) CuO-1, and b) CuO-2

The strong emission peak observed at approximately 322 nanometers was assigned to the near-blue-edge emission of the CuO product, indicating a blue shift to this peak as reported for CuO nanoPlatelets [21,22]. In general, the peaks with high and low intensity in the PL spectra indicated the faster and slower recombination of the electron-hole pair, respectively [23]. The peaks (as shoulder) observed at approximately 350 nanometers corresponded to the band-edge emission, and the broad peak at approximately 415 nanometers was due to artifact [24]. Finally, the broad peak at approximately 630 nanometers attributed to native defects [25]. These finding confirmed that the PL properties of the nanoparticles largely depended on the morphology and size of the nanoparticles [21].

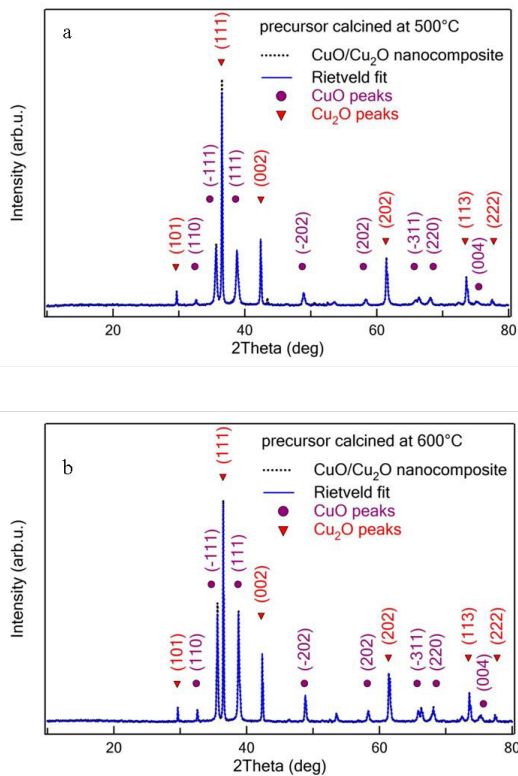


Fig 4. XRD patterns of a) CuO-1, and b) CuO-2

**XRD patterns**

Fig 4 depicts the XRD patterns of the prepared CuO/Cu<sub>2</sub>O nanocomposites (CuO-1 and CuO-2). The plane reflections observed at the 2θ values of 29.55 (101), 36.40 (111), 42.28 (002), 52.42 (112), 61.34 (202), 73.47 (113), and 77.32 (222) were indexed to the cubic phase of Cu<sub>2</sub>O with the JCPDS card number of 77-0199 [16] while the plane reflections observed at 32.47 (110), 35.52 (-111), 38.66 (111), 48.76 (-202), 53.38 (020), 58.19 (202), 61.53 (-113), 65.71 (022), 66.23 (-311), 72.30 (311), and 74.94 (004) were indexed to the monoclinic phase of CuO with the JCPDS card number of 89-5895 [16]. The structure was refined by the Rietveld fit in Jana2006 crystallographic program [27]. The fit could explain all the peaks, with the exception of two tiny peaks at 43.41 and 50.55 Cu-1 sample. As for the CuO-2 sample, no unexplained peak was observed. The unit cell parameters in both samples were found as a = 4.69 Å, b = 3.43 Å, c = 5.13 Å and β = 99.37° for monoclinic CuO and a = 4.27 Å for cubic Cu<sub>2</sub>O. By increasing the temperature from 500°C to 600°C, the phase fraction of CuO increased from 48.7% to 60.2%, while the phase fraction of Cu<sub>2</sub>O decreased

proportionally. The size of the crystallites was also calculated using the fundamental parameter approach [28] integrated in Jana2006, which eliminated the instrumental section of the diffraction pattern through the known geometry of the diffractometer. The mean crystallite size for the CuO nanoparticles prepared by the calcination of copper precursor at the temperature of 500°C was 41 (CuO) and 99 nanometers (Cu<sub>2</sub>O). As for the nanoparticles prepared by calcinations at the temperature of 600°C, the value was estimated at 72 (CuO) and 124 nanometers (Cu<sub>2</sub>O).

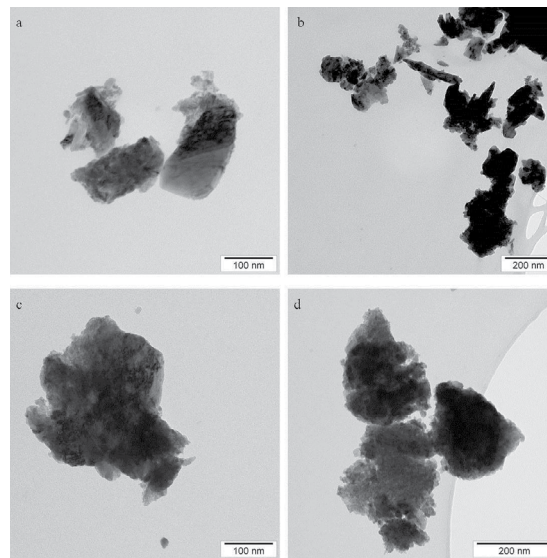


Fig 5. TEM images of a, b) CuO-1, and c, d) CuO-2 at various magnifications

**TEM images**

Fig 5 depicts the TEM images of the prepared CuO/Cu<sub>2</sub>O nanocomposites (CuO-1 and CuO-2). As can be seen, both products formed big clusters of particles with irregular shapes, which could not determine the size of the CuO and Cu<sub>2</sub>O crystallites. On the other hand, the clusters prepared by calcination at the temperature of 600°C evidently contained larger particles than the clusters prepared at the temperature of 500°C, which consistent with the results based on the XRD patterns.

**Antibacterial activity**

Fig 6 shows the antibacterial activity of the prepared CuO/Cu<sub>2</sub>O nanocomposites (CuO-1 and CuO-2) against two gram-positive and two gram-negative bacterial strains. In the current research, the CuO/Cu<sub>2</sub>O nanocomposites with

gentamicin were prepared as discs with the diameter of five millimeter based on the study by Moniri Javadhesari [26]. As is depicted in Fig-6, the maximum diameter of the inhibition zone belonged to *P. aeruginosa*. Moreover, the antibacterial effects of the prepared CuO/Cu<sub>2</sub>O nanocomposites against *E. coli* and *S. aureus* were notable, while the diameter of the inhibition zone around *B. cereus* was extremely low. According to our finding, the antibacterial activity sequence of the prepared CuO/Cu<sub>2</sub>O nanocomposites against the bacterial strains was as follows:

*P. aeruginosa* > *E. coli* > *S. aureus* > *B. cereus*

This finding is consistent with the antibacterial activity of CuO nanoparticles as reported by Moniri Javadhesari [26] and Nishino [29]. In the mentioned studies, the antibacterial activity of the CuO nanoparticles against *S. aureus* than *E. coli* was higher.

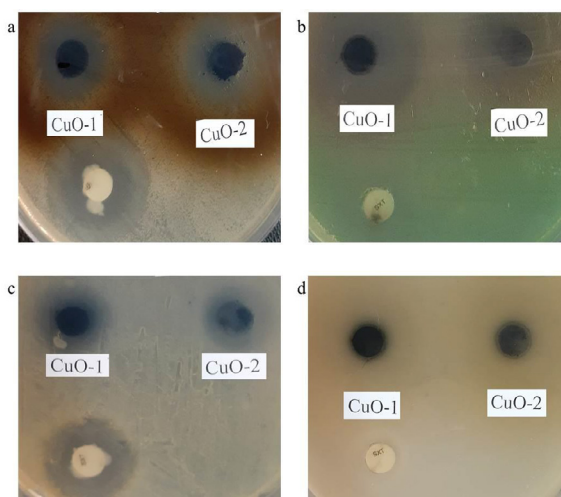


Fig 6. Inhibition zone of a) *E. coli*, b) *P. aeruginosa*, c) *S. aureus*, and d) *B. cereus*

## CONCLUSION

In this study, we prepared two CuO/Cu<sub>2</sub>O nanocomposites through the facile thermal decomposition of a new copper precursor at the temperature of 500°C and 600°C for 1.5 hours, which were characterized using various techniques. The FT-IR, XRD, and TEM techniques confirmed the formation of CuO/Cu<sub>2</sub>O nanocomposites with diverse shapes and high agglomeration. In addition, the UV-Vis and PL techniques confirmed the peaks regarding the direct transition of electrons and SPR. The antibacterial finding also indicated that the inhibitory effects of the CuO/Cu<sub>2</sub>O nanocomposites against two gram-negative bacterial strains were more significant compared

to the two gram-positive strains.

## ACKNOWLEDGMENTS

Hereby, we extend our gratitude to Golestan University and the Institute of Physics of the Czech Academy of Sciences for the financial support of this research project.

## REFERENCES

- Li Z, Mao Y, Tian Q, Zhang W, Yang L. Extremely facile preparation of high-performance Fe<sub>2</sub>O<sub>3</sub> anode for lithium-ion batteries. *J All Compd*. 2019; 784: 125-133.
- Al-Aoh H.A. Adsorption performances of nickel oxide nanoparticles (NiO NPs) towards bromophenol blue (BB). *Desal. Water Treat*. 2018; 110: 229-238.
- Jin K, Maalouf J.H., Lazouski N, Corbin N, Yang D, Manthiram Y. Epoxidation of cyclooctene using water as the oxygen atom source at manganese oxide electrocatalysts. *J Am Chem Soc*. 2019; 141: 6413-6418.
- Negi K, Kumar M, Singh G, Chauhan S, Chauhan M.S. Nanostructured CeO<sub>2</sub> for selective-sensing and smart photocatalytic application. *Deram Int*. 2018; 44: 15281-15289.
- Zhao C, Huang B, Zhou J, Xie E. Synthesis of porous Co<sub>3</sub>O<sub>4</sub> nanonetworks to detect toluene at low concentration. *Phys Chem Chem Phys*. 2014; 16: 19327-19332.
- Siddiqui H, Qureshi M.S., Haque F.Z. Surfactant assisted wet chemical synthesis of copper oxide (CuO) nanostructures and their spectroscopic analysis. *Optik*. 2016; 127: 2740-2747.
- Mohamed R.M, Harraz F.A, Shawky A. CuO nanobelts synthesized by a template-free hydrothermal approach with optical and magnetic characteristics. *Ceram Int*. 2014; 40: 2127-2133.
- Zhai X, Wang P, Yan Z, Ren N. Room temperature photoluminescence properties of CuO nanowire arrays. *Opt Mater*. 2015; 42: 544-547.
- Zhang L, Cui Z, Wu Q, Guo D, Xu Y, Guo L. Cu<sub>2</sub>O-CuO composite microframes with well-designed micro/nano structures fabricated via controllable etching of Cu<sub>2</sub>O microtubes for CO gas sensors. *Cryst Eng Commun*. 2013; 15: 7462-7467.
- Dong C, Zhong H, Kou T, Frenzel J, Eggeler G, Zhang Z. Three-dimensional Cu foam-supported single crystalline mesoporous Cu<sub>2</sub>O nanothorn arrays for ultra-highly sensitive and efficient nonenzymatic detection of glucose. *ACS Appl Mater Interfaces*. 2015; 7: 20215-20223.
- Wang P, Ng Y.H, Amal R. Embedment of anodized p-type Cu<sub>2</sub>O thin films with CuO nanowires for improvement in photoelectrochemical stability. *Nanoscale*. 2013; 5: 2952-2958.
- Sharmila G, Sakthi Pradeep R, Sandiya K, Santhiya S, Muthukumaran C, Jeyanthi J, Manoj Kumar N, Thitumarimurugan M. Biogenic synthesis of CuO nanoparticles using *Bauhinia tomentosa* leaves extract: Characterization and its antibacterial activities. *J Mol Struct*. 2018; 1165: 288-292.
- Fterich M, Nasr F.B, Lefi R, Toumi M, Guermazi S. Effect of concentration of hexamethylenetetramine in structure, microstructure and optical properties of CuO nanoparticles synthesized by hydrothermal route. *Mater Sci Semiconduct*

- Process. 2016; 43:114-122.
14. Rashad M, Al-Aoh H.A. Promising adsorption studies of bromophenol blue using copper oxide nanoparticles. *Desal Water Treat.* 2019; 139: 360-368.
  15. Lv J, Kong C, Xu Y, Yang Z, Zhang X, Yang S, Meng G, Bi J, Li J, Yang S. Facile synthesis of novel CuO/Cu<sub>2</sub>O nanosheets on copper foil for high sensitive nonenzymatic glucose biosensor. *Sensors and Actuators B Chem.* 2017; 248: 630–638.
  16. Yu L, Fedorov I.V, Karpov I.V, Ushakov A.V, Lepeshev A.A. Study of Phase Composition of CuO/Cu<sub>2</sub>O Nanoparticles Produced in the Plasma of a Low-Pressure Arc Discharge. *Inorg. Mater: Appl Res.* 2018; 9: 323–328.
  17. Sahu K, Satpati B, Singhal R, Mohapatra S. Enhanced catalytic activity of CuO/Cu<sub>2</sub>O hybrid nanowires for reduction of 4-nitrophenol in water. *J Phys Chem Solids .* 20; 136: 109143.
  18. Sharmila G, Thirumarimurgan M, Sivakumar V.M. Optical, catalytic and antibacterial properties of phytofabricated CuO nanoparticles using *Tecoma castanifolia* leaf extract. *Optik* 2016; 127: 7822-7828.
  19. Mageshwari K, Sathyamoorthy R. Flower-shaped CuO nanostructures: Synthesis, characterization and antimicrobial activity. *J Mater Sci Technol.* 2013; 29: 909-914.
  20. Liu X, Sui Y, Yang X, Jiang L, Wang F, Wei Y, Zou Z. A feasible approach to synthesize Cu<sub>2</sub>O microcrystals and their enhanced non-enzymatic sensor performance. *RSC Adv.* 2015; 5: 59099–59105.
  21. Uma Maheswari R, Jansi Rani B, Ravi G, Ruvakkumar R, Ameen F, Al-Sabri A. Structural, morphological, optical and antibacterial properties of pentagon CuO nanoplatelets. *J Sol-Gel Sci Technol.* 2018; 87: 515-527.
  22. Maji S.K, Mukherjee N, Mondal A, Adhikary B, Karmakar B. Chemical synthesis of mesoporous CuO from a single precursor: Structural, optical and electrical properties. *J Solid State Chem.* 2010;183:1900-19004.
  23. Senthil Kumar P, Selakumar M, Ganesh Babu S, Induja S, Karuthapandian S. CuO/ZnO nanorods: An affordable efficient p-n heterojunction and morphology dependent photocatalytic activity against organic contaminants. *J All Compd.* 2017; 701: 562-573.
  24. Tamuly C, Saikia I, Hazarika M, Das M.R. Reduction of aromatic nitro compounds catalyzed by biogenic CuO nanoparticles. *RSC Adv.* 2014; 4: 53229-53236.
  25. Shah M.A. A versatile route for the synthesis of nickel oxide nanostructures without organics at low temperature. *Nanoscale Res Lett.* 2008; 3: 255-259.
  26. Moniri Javadhesari S, Alipour S, Mohammadnejad S, Akbarpour M.R. Antibacterial activity of ultra-small copper oxide (II) nanoparticles synthesized by mechanochemical processing against *S. aureus* and *E. Coli*. *Mater Sci Eng C.* 2019; 105: 110011.
  27. Petricek V, Dusek M, Palatinus L. Crystallographic computing system JANA2006: General features. *Z Kristallogr.* 2014; 229: 345-352
  28. Cheary R.W, Coelho A.A. Axial divergence in a conventional X-ray powder diffractometer. II. Realization and evaluation in a fundamental-parameter profile fitting procedure. *J Appl Cryst.* 1998; 31: 862-868.
  29. Nishino F, Jeem M, Zhang L, Pkamoto K, Okabe S, Watanabe S. Formation of CuO nano-flowered surfaces via submerged photo-synthesis of crystallites and their antimicrobial activity. *Sci Rep.* 2017; 7:1063.